Metal-coordination-mediated sequential chelation-enhanced fluorescence (CHEF) and fluorescence resonance energy transfer (FRET) in a heteroditopic ligand system†

Robert J. Wandell, Ali H. Younes and Lei Zhu*

Received (in Montpellier, France) 31st March 2010, Accepted 4th May 2010
DOI: 10.1039/c0nj00241k

Sequential fluorescence enhancement and fluorescence resonance energy transfer over a zinc ion gradient have been engineered in a two-fluorophore heteroditopic ligand platform. This is the first report that the strategies of metal-coordination modulated photoinduced electron transfer (PET), internal charge transfer (ICT), and fluorescence resonance energy transfer (FRET) are integrated in one synthetic fluoroionophore. Comparing to the previously reported single-fluorophore heteroditopic ligands (L. Zhang, R. J. Clark and L. Zhu, *Chem. Eur. J.* 2008, **14**, 2894–2903), the resolution of two emission channels is greatly enhanced to almost 100 nm. This two-fluorophore heteroditopic platform lends promise to creating dual-emission fluorescent indicators where low- and high-target concentration regimes could be analyzed using independent emission filter sets.

Introduction

Controlling the relative preference of the relaxation pathways of an excited fluorophore by another substance is the basis for fluorescent sensing applications.[1–3] In most cases, changing the preference of two pathways (*i.e.* fluorescence *vs.* quenching) by an analyte results in a two-state switching of an optical signal (*i.e.* high *vs.* low intensity). The target concentration dependence of the readout is used to construct the calibration curve required for quantitative analysis. Multiple relaxation pathways, however, may be needed to satisfy more challenging situations, where the relative rates of those relaxation pathways of the excited fluorescent indicator molecule sensitively depend on the concentrations and identities of the analyte(s).

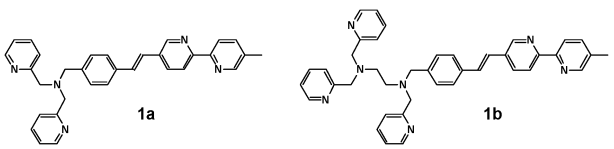

For example, we are interested in devising fluorescent ligand platforms based on which indicators effective over large analyte concentration ranges can be built.[4–6] In our first, one-fluorophore system such as compound **1a**,[4] a 2,2′-bipyridyl (bipy)-containing fluorophore capable of intramolecular charge transfer (ICT)[7] was coupled with a tridentate Zn^{2+}-binding dipicolylamino (DPA) group which suppresses fluorescence *via* photoinduced electron transfer (PET).[1,7] Using monotopic model compounds, the apparent dissociation constants of DPA and bipy to Zn^{2+} in CH_3CN were determined to be 0.3 μM and 1.3 μM, respectively.[4] Therefore, upon increasing the Zn^{2+} concentration ($[Zn^{2+}]$) in CH_3CN, the heteroditopic ligand (*i.e.* a ligand with two different metal ion binding sites) **1a** undergoes a chelation-enhanced fluorescence (CHEF) as the DPA group first binds Zn^{2+}.[8,9] When $[Zn^{2+}]$ is high enough to occupy the bipy site, the consequent stabilization of the charge-transfer excited state results in an emission bathochromic shift. Therefore, three fluorescence states (OFF, ON at λ_1, and ON at λ_2) of **1a**, which correlates to their respective coordination states, are accessible over a broad $[Zn^{2+}]$ gradient. The $[Zn^{2+}]$-dependent rate of the PET process and the energy of the ICT excited state determine the distribution of the three fluorescence states. Compound **1b** was later developed based on this design so that the $[Zn^{2+}]$-dependent distribution of the three fluorescence states was replicated under aqueous conditions.[10]

The one-fluorophore heteroditopic ligands such as **1a**, although effective in correlating three coordination states to three distinct fluorescence states, have their shortcomings. For example, the emission band separation ($\Delta\lambda = \lambda_2 - \lambda_1$) is 57 nm as measured in CH_3CN. Due to the solvatochromic nature of the fluorophore,[11] $\Delta\lambda$ decreases further for **1b** to 33 nm in aqueous solutions.[10] Therefore, it is challenging to find two emission filter sets for the two emission bands that are quite close to each other. The reported work is the first step towards creating dual-channel emission heteroditopic fluoroionophores that could be analyzed using two independent emission filter sets.

Results and discussion

Design

Motivated by the fact that a large separation of the two emission bands is challenging to achieve in the one-fluorophore heteroditopic system, we developed a two-fluorophore heteroditopic framework whose emission band separation

Department of Chemistry and Biochemistry, Florida State University, Tallahassee, FL 32306-4390, USA. E-mail: lzhu@chem.fsu.edu; Fax: +1 850 644 8281; Tel: +1 850 645 6813
† Electronic supplementary information (ESI) available: Syntheses, additional spectra, and procedures for measurements of fluorescence quantum yields and lifetimes. See DOI: 10.1039/c0nj00241k

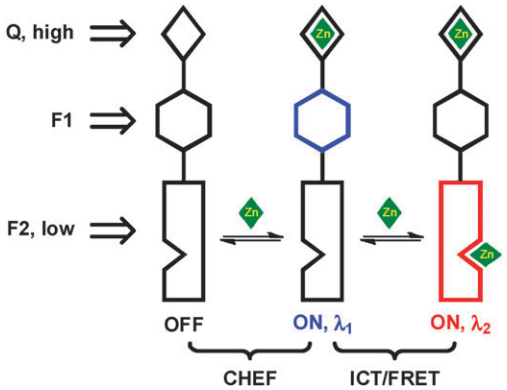

Fig. 1 Construct of a two-fluorophore heteroditopic ligand. Details in the text. Q: Quencher, also the high-affinity Zn^{2+} binding site; F1 and F2: fluorophores. F2 contains a low-affinity Zn^{2+} binding site. CHEF: CHelation-Enhanced Fluorescence; ICT: Internal Charge Transfer; FRET: Fluorescence Resonance Energy Transfer. The blue and red colors represent two different emission wavelengths (short and long).

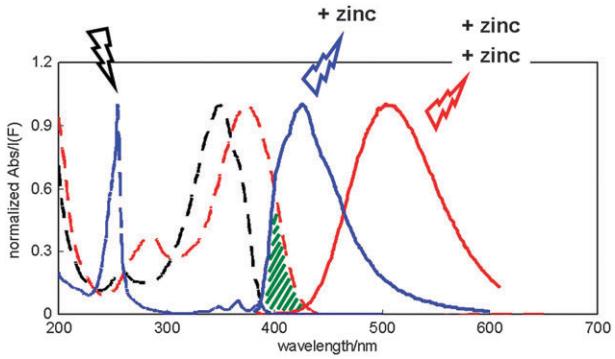

Fig. 3 Blue: spectra of $[Zn(\mathbf{2})]^{2+}$, red: spectra of $[Zn(\mathbf{3})]^{2+}$, and black: absorption spectrum of **3**. Dashed lines: absorption, solid lines: fluorescence. Black, blue and red lightning bolts represent the excitation of the engineered heteroditopic ligand, its emission at low and high $[Zn^{2+}]$, respectively.

may approach 100 nm. The designed two-fluorophore construct responds to an increasing $[Zn^{2+}]$ gradient *via* CHEF of the first fluorophore (F1, Fig. 1) followed by fluorescence resonance energy transfer (FRET) from the excited F1 to the second fluorophore (F2). The general operational principle is as the following: F1 is excited during the operation of the system. F2 undergoes charge transfer upon excitation. The high-affinity Zn^{2+} binding ligand (Q) quenches F1 *via* PET. Coordination of Zn^{2+} at the Q site shuts down the PET to restore the fluorescence in a typical CHEF manner. When Zn^{2+} is bound at F2, the charge-transfer excited state is stabilized to result in a bathochromic shift of the absorption spectrum, which enhances the spectral overlap with the emission of F1 and thus enables FRET from F1 to F2. Taken together, three fluorescence states (OFF, ON at λ_1, and ON at λ_2) can be achieved *via* the sequential CHEF and FRET processes over an increasing $[Zn^{2+}]$ gradient.

In this preliminary study, anthracene is selected as F1, and an ICT-capable thiophenevinyl-bipy (TVB) is F2. The spectral features of F1 and F2 were examined using model compounds **2** and **3** (Fig. 2 and 3). **2** which contains the tridentate DPA ligand undergoes a fluorescence-enhancing coordination with Zn^{2+} due to the CHEF effect.[12,13] An overlap (the green area in Fig. 3) between the absorption of **3** and the emission of $[Zn(\mathbf{2})]^{2+}$ is created when **3** binds Zn^{2+}. Consequently, when F1 is excited, FRET is likely to occur from the excited F1 to F2 to result in the emission from F2, if F1 and F2 were properly connected in one molecular scaffold.

By joining compounds **2** and **3** *via* an alkyl linker using the Cu(I)-catalyzed azide-alkyne "click" cycloaddition,[14,15] a two-fluorophore heteroditopic ligand **4** emerges (Scheme 1). Also designed were the monotopic compound **5**, which is a control without the high-affinity DPA chelating site, and the ditopic **6** which contains a shorter alkyl linker than that of **4**. Compound **6** is expected to be capable of a more efficient FRET than that of **4** because of a shorter interfluorophore distance.

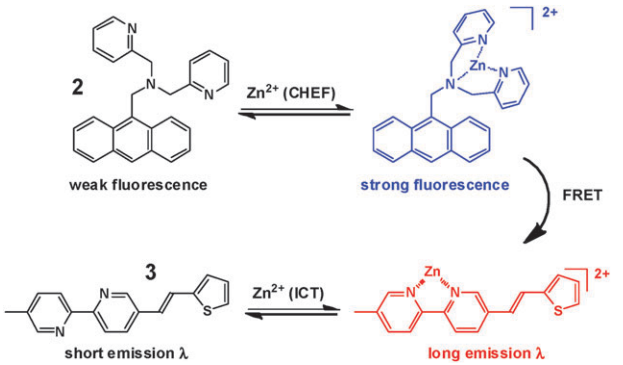

Fig. 2 The CHEF effect of **2** (top), the enhanced ICT of **3** upon Zn^{2+} coordination (bottom), and the engineerable FRET between the Zn^{2+} complexes of **2** and **3**.

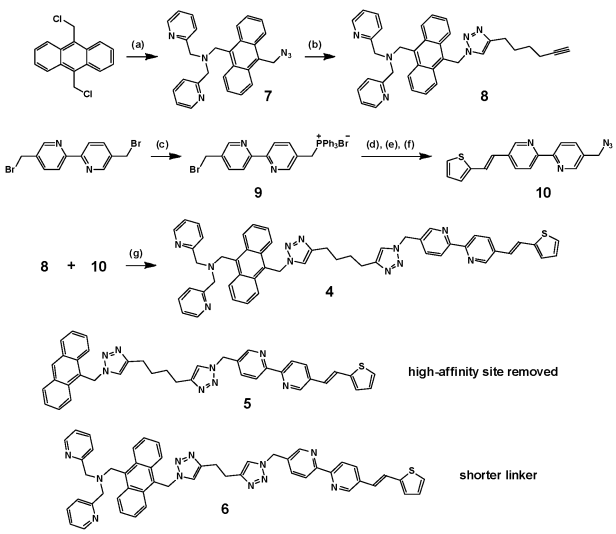

Scheme 1 (a) NaN_3, di-(2-picolyl)amine, Bu_4NI, 18-crown-6, rt, 37%; (b) 1,7-octadiyne, $Cu(OAc)_2$, sodium ascorbate, 38%; (c) Ph_3P, THF, 95%; (d) KHMDS, 2-thiophenecarboxaldehyde; (e) NaN_3; (f) I_2, CH_2Cl_2, 23% in 3 steps; (g) $Cu(OAc)_2$, sodium ascorbate, 32%.

Synthesis

The synthesis of **4** is shown in Scheme 1. Key to the sequence is the methods to desymmetrize the 9- and 10-positions of anthracene and 5- and 5′-positions of 2,2′-bipy. 9,10-dichloromethylanthracene undergoes a double-S_N2 substitution with 1 molar equivalent each of NaN_3 and di-(2-picolyl)amine to afford **7**, which is conveniently separated from the symmetrically substituted byproducts in 37% yield. "Clicking" of **7** with an excess amount of 1,7-octadiyne affords compound **8**. In parallel, monophosphonium salt **9** is prepared in a quantitative yield by treating 5,5′-dibromomethyl-2,2′-bipyridyl with triphenylphosphine in THF. The Wittig reaction between **9** and thiophenecarboxaldehyde followed by an S_N2 substitution with NaN_3 gives a *cis* and *trans* mixture of **10**. The crude product is treated with I_2 followed by chromatographic separation to afford pure *trans*-**10**. The click reaction between *trans*-**10** and **8** leads to the heteroditopic ligand **4**. The syntheses of **5** and **6** are described in the ESI.

Spectroscopic studies

The associations of **4–6** to Zn^{2+} were studied in spectroscopic titration experiments in CH_3CN. The respective dissociation constants of DPA and bipy sites to Zn^{2+} are expected to be close to the values determined using monotopic model compounds, 0.3 μM and 1.3 μM, respectively.[4] The absorption spectrum of **4** (blue in Fig. 4A) in CH_3CN is a composite of the three vibronic bands of **2** (dashed blue in Fig. 3) and maximum absorption band of **3** (dashed black in Fig. 3). With the addition of $Zn(ClO_4)_2$, the spectrum eventually undergoes a bathochromic shift due to the Zn^{2+}-coordination-mediated shift of the TVB component.[11] There is a short delay before the rise of the absorption at 396 nm upon increasing $[Zn^{2+}]$ (red isotherm in Fig. 4B). The delay of the bathochromic shift while $[Zn^{2+}]$ is increasing during the early stage of the titration is indicative of the preferential binding at the high-affinity DPA site.

The fluorescence spectrum of **4** shows desired features over a $[Zn^{2+}]$ gradient. The excitation wavelength is chosen at 260 nm to maximize the absorption of the anthryl group (FRET donor) and to minimize that of the TVB group (FRET acceptor).[16] A rapid growth of the anthryl emission is observed during the first leg of the Zn^{2+} titration followed by a red shift to the TVB emission (Fig. 5A). Importantly, the spectral separation of the two emission bands is ~90 nm, much larger than the 57 nm achieved using the one-fluorophore ligand **1a**. Presumably, the initial enhancement is resulted from a CHEF effect when

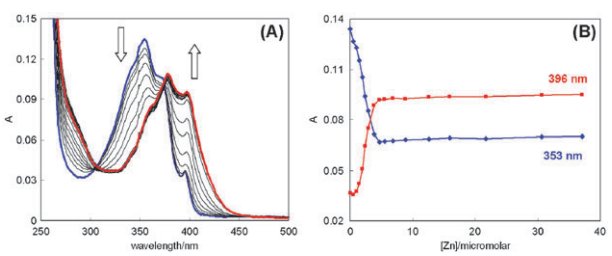

Fig. 4 (A) Absorption spectra of **4** (2.5 μM) in the presence of $Zn(ClO_4)_2$ from 0 (blue) to 37 μM (red) in CH_3CN. (B) The absorbance values of **4** at 353 nm and 396 nm at various $[Zn^{2+}]$.

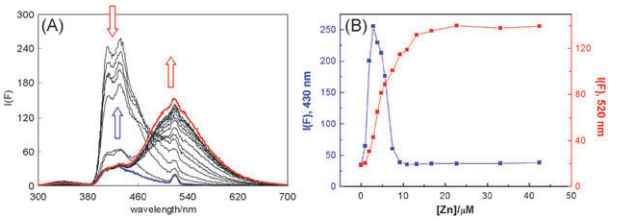

Fig. 5 (A) Fluorescence spectra of **4** (5.1 μM, λ_{ex} = 260 nm) in the presence of $Zn(ClO_4)_2$ from 0 (blue) to 74 μM (red) in CH_3CN. The band resulted from second-order scattering is seen at 520 nm. Blue arrow: the initial enhancement; red arrows: the following bathochromic shift. (B) The fluorescence intensity of **4** at 430 nm (blue) and 520 nm (red) at various $[Zn^{2+}]$.

Zn^{2+} binds at the DPA site in **4** and the later red shift is caused by FRET when TVB binds with Zn^{2+}. The intensity of anthryl emission at 430 nm rises quickly with increasing $[Zn^{2+}]$ before dropping back to the baseline (blue, Fig. 5B). On the other hand, the fluorescence enhancement at 520 nm is more gradual (red, Fig. 5B), indicating that the binding at TVB lags behind the coordination at the DPA site. The quenching of the anthryl emission during the second leg of the titration experiment strongly suggests that FRET is taking place from the excited anthryl group to Zn^{2+}-bound TVB group, as supported by the evidence described in the next paragraph. Compound **5**, which does not have a DPA site on the anthryl group, does not experience an initial ascent in the anthryl fluorescence (Fig. S2†). Instead, a bathochromic shift occurs immediately upon the addition of $Zn(ClO_4)_2$, consistent with the coordination at the TVB site which results in FRET.

The occurance of FRET from the anthryl group to the TVB site in **4** is supported by the following control experiment. A sample containing both model anthryl and TVB compounds **2** and **3** was excited at 260 nm and the flureoscence was observed as $[Zn^{2+}]$ was increased to over 3 molar equivalents of the total ligand concentration (6 μM). A large enhancement in anthryl fluorescence was observed during the early stage of the titration, after which the change in emission is minimal (Fig. 6).[17] The lack of quenching of anthryl fluorescence and the small amplitude of the emission of **4** when coordination of Zn^{2+} with **4** occurs supports the rationale that a FRET

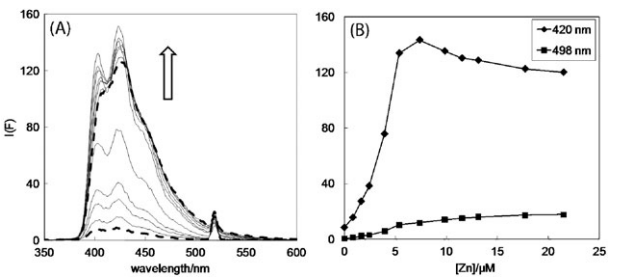

Fig. 6 (A) Fluorescence spectra (λ_{ex} = 260 nm) of the mixture of **2** (3 μM) and **3** (3 μM) in the presence of $Zn(ClO_4)_2$ from 0 to 21 μM in CH_3CN. The dashed lines represent the first and last spectra collected during the titration experiment. The arrow indicates the spectral evolution upon increasing $[Zn^{2+}]$. The band resulted from second-order scattering is seen at 520 nm. (B) The fluorescence intensity of the mixed sample at 420 nm (diamonds) and 498 nm (squares) at various $[Zn^{2+}]$.

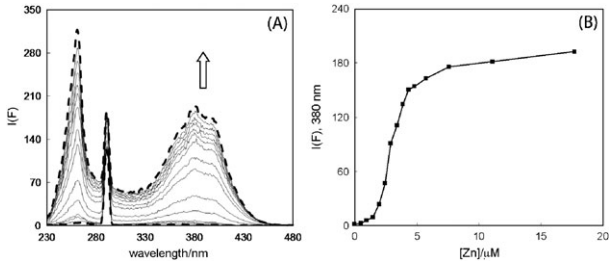

Fig. 7 (A) Excitation spectra (λ_{em} = 580 nm) of **4** (4.9 μM) in the presence of $Zn(ClO_4)_2$ (0–18 μM) in CH_3CN. The sharp band of second-order scattering is seen at 290 nm. The dashed lines represent the first and last spectra collected during the titration experiment. The arrow indicates the spectral evolution upon increasing [Zn^{2+}]. (B) Fluorescence intensity (580 nm) values excited at 380 nm *vs.* the concentration of $Zn(ClO_4)_2$.

Table 1 Maximum emission wavelengths, fluorescence quantum yields (ϕ_f), and lifetimes (τ),[a] of **4–6** and their Zn^{2+} complexes in CH_3CN

	λ_{em}/nm	ϕ_f	τ (avg)/ns
4	424	0.023	3.05
$[Zn(\mathbf{4})]^{2+}$	410, 428[b]	0.15	ND
$[Zn_2(\mathbf{4})]^{4+}$	514	0.13	5.99
5	432	0.085	1.70
$[Zn(\mathbf{5})]^{2+}$	513	0.043	2.47
6	428	0.016	5.36
$[Zn(\mathbf{6})]^{2+}$	411, 428[b]	0.098	ND
$[Zn_2(\mathbf{6})]^{4+}$	515	0.21	5.68

[a] Fluorescence decay traces of free ligands and Zn^{2+} complexes were observed at 431 nm and 517 nm, respectively. A 370 nm LED was used as the excitation source. ND: not determined. [b] Two emission vibronic bands with similar intensity were recorded.

process is only allowed to proceed when **2** and **3** are covalently linked to afford compound **4**, where the occurance of acceptor emission (TVB-Zn^{2+}) is accompanied by the quenching of the donor emission (anthryl).

Monitored at 580 nm where the Zn^{2+}-bound TVB emits exclusively, the excitation spectra of **4** (Fig. 7) collected at various [Zn^{2+}] lack the mirror image relationship with the corresponding fluorescence spectra and resemble the absorption spectra of **4**. This observation is consistent with a sensitized (*e.g.* excited *via* energy transfer) rather than a direct excitation of the Zn^{2+}-bound TVB moiety. The delayed appearance of the emission at 580 nm from the Zn^{2+}-bound TVB site is reflected in the sigmoidal shape of the titration isotherm (Fig. 7B). The Zn^{2+} added during the early stage of the titration was absorbed by the high-affinity DPA site which results in the fluorescence at the shorter wavelength 420 nm.

FRET efficiency is highly sensitive to the distance between the donor and acceptor fluorophores in addition to their spectral overlap. Compound **6**, which has a shorter alkyl linker between its two fluorophores, behaves similarly to **4** in fluorescence titration experiments (Fig. 8A), except that the quenching of the anthryl fluorescence upon Zn^{2+}-binding at the TVB site in **6** is more complete than that of **4**. This observation further corroborates the FRET hypothesis.

An excitation wavelength within the near UV or visible range is desirable for applications such as live-cell imaging, because background fluorescence can be reduced. When **6** was excited at 375 nm, similar fluorescence response to Zn^{2+} was observed (Fig. 8B). However under this condition, both FRET (judging by the quenching of anthryl emission) and direct excitation contribute to the fluorescence of TVB. The titration data of compounds **4** and **5** with excitation at 375 nm are shown in Fig. S3–S4†.

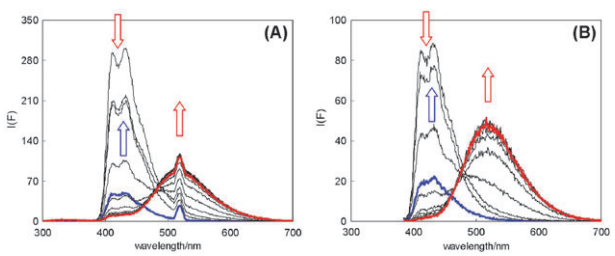

Fig. 8 (A) Fluorescence spectra of **6** (5.1 μM, λ_{ex} = 260 nm) in the presence of $Zn(ClO_4)_2$ from 0 (blue) to 74 μM (red) in CH_3CN. (B) Fluorescence spectra of **6** (4.9 μM, λ_{ex} = 375 nm) in the presence of $Zn(ClO_4)_2$ from 0 (blue) to 32 μM (red).

The fluorescence quantum yields of **4** and **6** increase upon forming mono- and dizinc complexes (Table 1). Zn^{2+}-binding is expected to reduce the rates of nonradiative decay processes because (1) the binding at the DPA group removes the nonradiative PET, and (2) the coordination at the TVB site rigidifies the structure of the fluorophore.[11] Excited by a 370 nm LED, the fluorescence decay traces of all the species collected using the Time-Correlated Single-Photon Counting (TCSPC) method can be fitted using three exponentials (Table S1†, Fig. S11–S12†). Due to the presence of flexible alkyl linker units in **4–6**, multiple conformations could be accessed in the excited states. Hence, in this preliminary report, we do not attempt to establish specific molecular models accounting for each lifetime (τ) component without additional experimental data. The average fluorescence lifetimes† were calculated. The values for the dizinc complexes of **4** and **6** (5.99 ns, 5.68 ns), which were determined at the emission band of the TVB component, are much higher than the τ of the Zn^{2+} complex of the model compound **3** (1.91 ns).[11] This observation is consistent with the involvement of a sensitized excitation of the TVB fluorophore operated *via* resonance energy transfer.

The preliminary study on metal ion selectivity was carried out using **6** in MeCN. The nitrogen-based DPA and bipy ligands are known to bind first-row transition metal ions with much higher affinities than alkali (Group 1) and alkaline earth (Group 2) metal ions. As expected, compound **6** coordinates Cu^{2+}, Cd^{2+}, and Pb^{2+} in a sequential fashion (Fig. S6–S8†) similar to the binding with Zn^{2+}. The absorption spectrum of **4** undergoes bathochromic shift at high Cu^{2+}/Cd^{2+}/Pb^{2+} concentration due to the coordination at the charge-transfer chromophore TVB site. Cd^{2+} and Pb^{2+} have similar effects on the fluorescence of **6** to that of Zn^{2+}, where an enhancement is followed by a bathochromic shift over an increasing metal ion gradient. Cu^{2+} quenches the fluorescence of **6** efficiently due to its paramagnetic nature. Alkali metal ions Ca^{2+} and Mg^{2+}, on the other hand, show minimal impact on the fluorescence of **6** (Fig. S9–S10†).

Conclusions

In summary, a two-fluorophore heteroditopic ligand system is established which is capable of achieving three different fluorescence states over a [Zn^{2+}] gradient. With increasing [Zn^{2+}], sequential CHEF (termination of the PET process) and enhanced ICT-enabled FRET occur which gives rise to a fluorescence enhancement followed by a bathochromic shift. This work may lead to improved fluorescent indicators for Zn^{2+} that are effective over broad concentration ranges, which is a primary interest of our laboratory.[10,18–20]

Most small molecule-based zinc indicators reported to date[21–25] utilize either photoinduced electron transfer (PET),[26–32] internal charge transfer (ICT),[33–35] or excited-state proton transfer (ESPT)[36] as the basis for zinc-induced fluorescence switch mechanism. Despite having been applied in designing sacrificial indicators for hydrolytic enzymes,[37–40] the FRET mechanism in devising fluorescent indicators for Zn^{2+} is under-exploited.[41] Lately, FRET has begun to be incorporated in the development of synthetic fluorescent indicators for small molecular analytes.[42–47] We report herein for the first time where the strategies of metal-coordination-modulated PET, ICT, and FRET are integrated in one synthetic fluoroionophore. The uniquely attractive feature of the two-fluorophore design comparing to our prior one-fluorophore-based heteroditopic ligands is that the separation of the two emission bands can be as large as 90 nm. This expanded separation of two emission wavelength channels may enable the use of matching emission filter sets for each fluorophores in and hence simplify biological imaging applications using dual-channel fluorescence. The fluorescence responses of the reported system to the [Zn^{2+}] gradient are the direct consequence of fast, reversible metal coordination interactions, which promises the application of our system in real-time imaging applications after structural refinements targeting specific situations.

This work was supported by FSU, a New Investigator Research (NIR) grant from the James and Esther King Biomedical Research Program administered by the Florida Department of Health (08KN-16), and the National Science Foundation (CHE0809201). We thank Manuel Constantino for assistance in synthesis.

Experimental

Synthesis of compound 4

Compound 7. 9,10-Bis(chloromethyl)anthracene (2 mmol, 550 mg) was dissolved in DMF (40 mL) followed by sequential addition of diisopropylethylamine (8.0 mmol, 1.4 mL), NaN_3 (2.0 mmol, 130 mg), di-(2-picolyl)amine (2.0 mmol, 360 μL), 18-crown-6 (catalytic amount), and tetrabutylammonium iodide (catalytic amount). The reaction was stirred at rt for 16 h before DMF was removed under vacuum. The residue was diluted with toluene followed by extraction with a NaOH solution (0.5 M, saturated with NaCl, aka "basic brine") for three times. The organic fraction was dried over K_2CO_3 before the solvent was removed under vacuum. The crude product was analyzed by TLC (alumina, ethyl acetate as eluent, R_f = 0.5). Compound **7** was isolated by alumina chromatography eluted by 10–30% ethyl acetate in CH_2Cl_2. The yield was 37%. ^{1}H NMR (300 MHz, $CDCl_3$): δ/ppm 8.42 (m, 4H), 8.21 (d, J = 8.4 Hz, 2H), 7.50 (m, 6H), 7.25 (m, 2H), 7.03 (m, 2H), 5.22 (s, 2H), 4.62 (s, 2H), 3.82 (s, 4H). ^{13}C NMR (75 MHz, $CDCl_3$): δ/ppm 159.5, 148.7, 136.1, 132.3, 131.2, 130.3, 126.5, 126.2, 126.0, 125.3, 123.9, 123.5, 122.0, 60.6, 51.0, 46.5. HRMS (ESI+): calcd. ($M + H^+$) 445.2141, found 445.2128.

Compound 8. Compound **7** (0.31 mmol, 138 mg) and 1,7-octadiyne (1.55 mmol, 206 μL) were dissolved in CH_3OH (17 mL). Aqueous solutions of sodium ascorbate (0.5 M, 1 mL) and $Cu(OAc)_2$ (0.1 M, 1 mL) were mixed to produce an orange suspension containing the Cu(I) catalytic species, which was subsequently added to the stirring methanolic solution. The mixture was stirred for 2 days followed by the addition of an aqueous solution of EDTA (0.1 M, 2 mL) while the stirring was continued for 1 h. Most of CH_3OH was subsequently removed under vacuum. The residue was partitioned between ethyl acetate and the basic brine. The organic fraction was washed with the basic brine two more times before dried over K_2CO_3. The solvent was removed, and Compound **8** was isolated by alumina chromatography eluted by 20–50% ethyl acetate in CH_2Cl_2. The yield was 38%. ^{1}H NMR (300 MHz, $CDCl_3$): δ/ppm 8.50 (d, J = 9.5 Hz, 2H), 8.47 (d, J = 4.3 Hz, 2H), 8.26 (d, J = 8.4 Hz, 2H), 7.54 (m, 6H), 7.29 (d, J = 7.8 Hz, 2H), 7.11 (m, 2H), 5.28 (s, 2H), 4.70 (s, 2H), 3.90 (s, 4H). ^{13}C NMR (75 MHz, $CDCl_3$): δ/ppm 159.4, 148.7, 136.2, 132.3, 131.2, 130.3, 126.5, 126.0, 125.3, 123.9, 123.5, 122.0, 60.6, 50.8, 46.5. HRMS (ESI+): calcd. ($M + H^+$) 551.2923, found 551.2917.

Compound 10. A flame-dried flask was charged with dry THF (25 mL) and **9**[4] (1.42 g, 2.35 mmol) and cooled to −78 °C. Thiophenecarboxaldehyde (0.43 mL, 4.70 mmol) and potassium bis(trimethylsilyl)amide (4.70 mL, 0.5 M in toluene, 2.35 mmol) were added dropwise sequentially. The mixture turned bright reddish after stirring for 20 min, after which the temperature was slowly raised to rt in 2 h. The reaction mixture was poured into icy brine and extracted with ethyl acetate (25 mL × 4). The combined organic portions were washed with brine, dried over Na_2SO_4, filtered and concentrated, to afford a reddish oil. The ^{1}H NMR was taken to verify the formation of the olefin product. The crude product was used directly in the next reaction without purification.

The crude olefin product (460 mg, 1.29 mmol) from the previous step was dissolved in THF (20 mL). NaN_3 (160 mg, 2.58 mmol), tetrabutylammonium iodide (catalytic amount), and 18-crown-6 (catalytic amount) were added sequentially. The reaction mixture was stirred for overnight at rt. The reaction mixture was poured into water and extracted with CH_2Cl_2 (25 mL × 4). The combined organic portions were washed with water and dried over Na_2SO_4 and filtered. After solvent removal, a ^{1}H NMR of the residue was taken to verify the formation of the azido product. The crude product was used directly in the next step without further purification.

The crude azido product **10** from the previous step was dissolved in CH_2Cl_2 (15 mL). Iodine (360 mg, 1.25 mmol) was added. The reaction mixture, protected from ambient light by aluminum foil, was stirred overnight at rt before poured into

water and extracted with CH_2Cl_2 (25 mL × 4). The combined organic portions were washed with water and dried over Na_2SO_4 before solvent was removed. The crude product was purified using silica chromatography eluted with ethyl acetate in CH_2Cl_2 (gradient 0–30%). The yield for the three-step sequence is 23%. ^{1}H NMR (300 MHz, $CDCl_3$): δ/ppm 8.73 (d, J = 2.1 Hz, 1H), 8.63 (d, J = 1.8 Hz, 1H), 8.44 (d, J = 8.4 Hz, 1H), 8.39 (d, J = 8.4 Hz, 1H), 7.94 (dd, J = 2.1, 8.4 Hz, 1H), 7.80 (dd, J = 2.1, 8.4 Hz, 1H), 7.37 (d, J = 15.9 Hz, 1H), 7.27 (m, 1H), 7.15 (d, J = 3.3 Hz, 1H), 7.04 (dd, J = 3.6, 5.1 Hz, 1H), 6.95 (d, J = 16.2 Hz, 1H), 4.55 (s, 2H). ^{13}C NMR (75 MHz, $CDCl_3$): δ/ppm 156.0, 154.4, 148.9, 148.0, 142.3, 136.8, 133.3, 133.1, 131.1, 127.9, 127.2, 125.5, 124.2, 121.1, 52.2. HRMS (ESI+): calcd. ($M + H^+$) 320.0970, found 320.0980.

Compound 4. Compounds **8** (20 mg, 0.354 mmol) and **10** (11 mg, 0.354 mmol) were dissolved in CH_3OH (2 mL). Aqueous solutions of sodium ascorbate (0.5 M, 1 mL) and $Cu(OAc)_2$ (0.1 M, 1 mL) were mixed to produce an orange suspension containing the Cu(I) catalytic species. The orange Cu(I) suspension (0.23 mL) was added to the stirring mixture. The mixture was stirred for overnight at rt followed by the addition of an EDTA solution (0.5 M, 0.23 mL) while the stirring was continued for 1 h. The solvent was subsequently removed under vacuum. The residue was diluted with ethyl acetate, washed with basic brine (pH = 12, 30 mL × 3), then dried over K_2CO_3. The solvent was removed and compound **4** was isolated by alumina chromatography eluted by ethyl acetate followed by 1–4% CH_3OH in CH_2Cl_2. The compound was further purified by washing with diethyl ether. The yield was 32%. ^{1}H NMR (300 MHz, $CDCl_3$): δ/ppm 8.72 (s, 1H), 8.54 (m, 5H), 8.38 (t, J = 8.3 Hz, 2H), 8.28 (d, J = 8.6 Hz, 2H), 7.92 (d, J = 8.1 Hz, 1H), 7.67 (d, J = 8.3 Hz, 1H), 7.61–7.48 (m, 6H), 7.39–7.26 (m, 4H), 7.18–7.10 (m, 4H), 7.04 (t, J = 4.2 Hz, 1H), 6.93 (d, J = 16.1 Hz, 1H), 6.82 (s, 1H), 6.44 (s, 2H), 5.52 (s, 2H), 4.73 (s, 2H), 3.90 (s, 4H), 2.62 (t, J = 7.2 Hz, 2H), 2.52 (t, J = 7.0 Hz, 2H), 1.59 (m, 4H). ^{13}C NMR (75 MHz, $CDCl_3$): δ/ppm 159.3, 156.4, 154.0, 148.8, 148.7, 148.5, 148.0, 147.9, 142.2, 136.6, 136.3, 133.2, 131.3, 130.5, 130.4, 127.8, 127.2, 127.0, 126.2, 125.5, 125.4, 124.7, 124.2, 124.1, 123.5, 122.1, 121.2, 121.1, 120.5, 120.2, 60.5, 51.3, 51.0, 46.5, 41.0, 28.8, 25.4, 25.3. HRMS (ESI+): calcd. ($M + H^+$) 870.3815, found 870.3827.

Procedure for spectroscopic studies. The spectroscopic titration experiments were carried out following a procedure that was published by our group.[4,20] Briefly, the absorption spectrum of an CH_3CN solution of a ligand in a semi-micro quartz spectrophotometer cuvette (Starna®) was recorded in the 200–600 nm range after baseline correction. Increments of $Zn(ClO_4)_2$ solution in CH_3CN was titrated into the cuvette and spectra were collected until no further spectral change was observed. Over the course of a titration experiment, the total concentration of the ligand was kept constant.

Same titration method was applied in the acquisition of the fluorescence spectra. The sample was excited at two different wavelengths, 260 and 375 nm, contigent upon the design of the experiments.

Notes and references

1 A. P. de Silva, H. Q. N. Gunaratne, T. Gunnlaugsson, A. J. M. Huxley, C. P. McCoy, J. T. Rademacher and T. E. Rice, *Chem. Rev.*, 1997, **97**, 1515–1566.
2 J. R. Lakowicz, in *Principles of Fluorescence Spectroscopy*, Springer, 2006, ch. 19, Fluorescence Sensing.
3 B. Valeur, in *Molecular Fluorescence. Principles and Applications*, Wiley-VCH, 2002, ch. 10, Fluorescent Molecular Sensors of Ions and Molecules.
4 L. Zhang, R. J. Clark and L. Zhu, *Chem.–Eur. J.*, 2008, **14**, 2894–2903.
5 L. Zhang and L. Zhu, *J. Org. Chem.*, 2008, **73**, 8321–8330.
6 L. Zhu, L. Zhang and A. H. Younes, *Supramol. Chem.*, 2009, **21**, 268–283.
7 B. Valeur and I. Leray, *Coord. Chem. Rev.*, 2000, **205**, 3–40.
8 M. E. Huston, K. W. Haider and A. W. Czarnik, *J. Am. Chem. Soc.*, 1988, **110**, 4460–4462.
9 E. U. Akkaya, M. E. Huston and A. W. Czarnik, *J. Am. Chem. Soc.*, 1990, **112**, 3590–3593.
10 L. Zhang, C. S. Murphy, G.-C. Kuang, K. L. Hazelwood, M. H. Constantino, M. W. Davidson and L. Zhu, *Chem. Commun.*, 2009, 7408–7410.
11 A. H. Younes, L. Zhang, R. J. Clark and L. Zhu, *J. Org. Chem.*, 2009, **74**, 8761–8772.
12 S. A. de Silva, A. Zavaleta, D. E. Baron, O. Allam, E. V. Isidor, N. Kashimura and J. M. Percapio, *Tetrahedron Lett.*, 1997, **38**, 2237–2240.
13 A. P. de Silva, T. S. Moody and G. D. Wright, *Analyst*, 2009, **134**, 2385–2393.
14 V. V. Rostovtsev, L. G. Green, V. V. Fokin and K. B. Sharpless, *Angew. Chem., Int. Ed.*, 2002, **41**, 2596–2599.
15 M. Meldal and C. W. Tornøe, *Chem. Rev.*, 2008, **108**, 2952–3015.
16 Excitation of the control compound **3** (TVB) and its Zn^{2+} complex at 260 nm results in much weaker fluorescence than that *via* excitation at 375 nm (Fig. S1†).
17 The slight emission reduction at 420 nm and concomittant enhancement at 498 nm (Fig. 6B) is ascribed to the bathochromic shift of the inefficiently excited **3** upon Zn^{2+} binding. When a longer excitation wavlength (345 nm) was employed, the fluorescence of $[Zn(\mathbf{3})]^{2+}$ was stronger, however, without quenching of the anthryl emission (Fig. S5†).
18 L. Zhang, S. Dong and L. Zhu, *Chem. Commun.*, 2007, 1891–1893.
19 S. Huang, R. J. Clark and L. Zhu, *Org. Lett.*, 2007, **9**, 4999–5002.
20 H. A. Michaels, C. S. Murphy, R. J. Clark, M. W. Davidson and L. Zhu, *Inorg. Chem.*, 2010, **49**, 4278–4287.
21 P. Jiang and Z. Guo, *Coord. Chem. Rev.*, 2004, **248**, 205–229.
22 K. Kikuchi, H. Komatsu and T. Nagano, *Curr. Opin. Chem. Biol.*, 2004, **8**, 182–191.
23 Z. Dai and J. W. Canary, *New J. Chem.*, 2007, **31**, 1708–1718.
24 E. L. Que, D. W. Domaille and C. J. Chang, *Chem. Rev.*, 2008, **108**, 1517–1549.
25 E. M. Nolan and S. J. Lippard, *Acc. Chem. Res.*, 2009, **42**, 193–203.
26 M. Royzen, A. Durandin, V. G. J. Young, N. E. Geacintov and J. W. Canary, *J. Am. Chem. Soc.*, 2006, **128**, 3854–3855.
27 R. Parkesh, T. C. Lee and T. Gunnlaugsson, *Org. Biomol. Chem.*, 2007, **5**, 310–317.
28 X.-a. Zhang, D. Hayes, S. J. Smith, S. Friedle and S. J. Lippard, *J. Am. Chem. Soc.*, 2008, **130**, 15788–15789.
29 W. Jiang, Q. Fu, H. Fan and W. Wang, *Chem. Commun.*, 2008, 259–261.
30 F. Qian, C. Zhang, Y. Zhang, W. He, X. Gao, P. Hu and Z. Guo, *J. Am. Chem. Soc.*, 2009, **131**, 1460–1468.
31 Z. Xu, G.-H. Kim, S. J. Han, M. J. Jou, C. Lee, I. Shin and J. Yoon, *Tetrahedron*, 2009, **65**, 2307–2312.
32 Z. Xu, K.-H. Baek, H. N. Kim, J. Cui, X. Qian, D. R. Spring, I. Shin and J. Yoon, *J. Am. Chem. Soc.*, 2010, **132**, 601–610.
33 A. Ajayaghosh, P. Carol and S. Sreejith, *J. Am. Chem. Soc.*, 2005, **127**, 14962–14963.
34 S. Sumalekshmy, M. M. Henary, N. Siegel, P. V. Lawson, Y. Wu, K. Schmidt, J.-L. Bredas, J. W. Perry and C. J. Fahrni, *J. Am. Chem. Soc.*, 2007, **129**, 11888–11889.
35 K. Komatsu, Y. Urano, H. Kojima and T. Nagano, *J. Am. Chem. Soc.*, 2007, **129**, 13447–13454.

36 M. M. Henary, Y. Wu and C. J. Fahrni, *Chem.–Eur. J.*, 2004, **10**, 3015–3025.
37 E. D. Matayoshi, G. T. Wang, G. A. Krafft and J. Erickson, *Science*, 1990, **247**, 954–958.
38 Y. Kawanishi, K. Kikuchi, H. Takakusa, S. Mizukami, Y. Urano, T. Higuchi and T. Nagano, *Angew. Chem. Int. Ed.*, 2000, **39**, 3438–3440.
39 H. Takakusa, K. Kikuchi, Y. Urano, H. Kojima and T. Nagano, *Chem.–Eur. J.*, 2003, **9**, 1479–1485.
40 O. Wichmann, J. Wittbrodt and C. Schultz, *Angew. Chem., Int. Ed.*, 2006, **45**, 508–512.
41 C. C. Woodroofe and S. J. Lippard, *J. Am. Chem. Soc.*, 2003, **125**, 11458–11459.
42 B. Valeur, J. Pouget, J. Bourson, M. Kaschke and N. P. Ernesting, *J. Phys. Chem.*, 1992, **96**, 6545–6549.
43 F. Bolletta, I. Costa, L. Fabbrizzi, M. Liccelli, M. Montalti, P. Pallavicini, L. Prodi and N. Zaccheroni, *J. Chem. Soc., Dalton Trans.*, 1999, 1381–1385.
44 S. H. Lee, S. K. Kim, J. H. Bok, S. H. Lee, J. Yoon, K. Lee and J. S. Kim, *Tetrahedron Lett.*, 2005, **46**, 8163–8167.
45 M. H. Lee, H. J. Kim, S. Yoon, N. Park and J. S. Kim, *Org. Lett.*, 2008, **10**, 213–216.
46 X. Zhang, Y. Xiao and X. Qian, *Angew. Chem.,Int. Ed.*, 2008, **47**, 8025–8029.
47 M. Suresh, S. Mishra, S. K. Mishra, E. Suresh, A. K. Mandal, A. Shrivastav and A. Das, *Org. Lett.*, 2009, **11**, 2740–2743.

